Silsesquioxane–Based Nanoparticles Formed via Hydrolytic Condensation of Organotriethoxysilane Containing Hydroxy Groups

ARTICLE *in* MACROMOLECULES · JULY 2004

Impact Factor: 5.8 · DOI: 10.1021/ma035482o

4 AUTHORS, INCLUDING:

Axel H E Mueller
Johannes Gutenberg-Universität Mainz
590 PUBLICATIONS **17,847** CITATIONS
SEE PROFILE

Joachim E. Klee
Dentsply De Trey
126 PUBLICATIONS **684** CITATIONS
SEE PROFILE

Silsesquioxane-Based Nanoparticles Formed via Hydrolytic Condensation of Organotriethoxysilane Containing Hydroxy Groups

Hideharu Mori,*,† Michael G. Lanzendörfer,‡ and Axel H. E. Müller

Lehrstuhl für Makromolekulare Chemie II, and Bayreuther Zentrum für Kolloide und Grenzflächen, Universität Bayreuth, D-95440 Bayreuth, Germany

Joachim E. Klee

Dentsply DeTrey GmbH, De-Trey-Strasse 1, D-78467 Konstanz, Germany

Received October 1, 2003; Revised Manuscript Received April 22, 2004

ABSTRACT: Silsesquioxanes-based nanoparticles synthesized by hydrolytic condensation of a functionalized precursor, *N*,*N*-di(2,3-dihydroxypropyl)(aminopropyl)triethoxysilane, $(HOCH_2CH(OH)CH_2)_2NCH_2CH_2CH_2Si(OCH_2CH_3)_3$, were characterized using MALDI-TOF MS, NMR, elemental analysis, FT-IR, transmission electron microscopy (TEM), and scanning force microscopy (SFM). MALDI-TOF MS analysis indicated that the product consists of many species having 12−18 Si atoms with different numbers of intramolecular cyclizations, and Si−O−C bonds are formed through the reaction of SiOH (or SiOEt) groups with the hydroxyl functionalities of an organic moiety bonded to a Si atom. The species having high number of intermolecular cyclization ($f \geq 0.5$ at $10 \geq n \geq 7$) were predominantly detected, suggesting that the product mainly consists of complete and incomplete cagelike structures. The chemical composition of the product was consistent with that calculated from the structure, $(R-SiO_{1.5})_n$, indicating that the nanoparticles belong to a family of silsesquioxanes characterized by a ratio of 1.5 between the silicon and oxygen atoms. Reasonable NMR and FT-IR spectra were observed, corresponding to the structure assuming that majority of the alkyl chain attached on a Si atom was intact during the hydrolytic condensation. The resulting particles have relatively narrow size distribution with average particle diameter less than 3.0 nm, as confirmed by TEM and SFM.

Introduction

Organic−inorganic hybrid nanoparticles have attracted a great deal of attention because of their potential applications in optics, electronics, engineering, and biosciences. Further advances of such organic−inorganic nanocomposite materials require fine-tuning of the sizes, structures, compositions, topologies, and spatial assembly of individual constitutes and their interfaces.[1] Recently, we developed novel intelligent colloidal polymer/silica nanocomposites in which the complexation of tertiary amine-containing silica nanoparticles and a weak anionic polyelectrolyte, poly(acrylic acid), can be manipulated simply by pH change in aqueous solution through hydrogen-bonded interaction and ionic complexation caused by hydrogen-transfer interactions between the constituents.[2] To provide an effective route for the controlled self-ordering of nanoparticles with polymers and for the achievement of characteristic stimuli-responsive properties in aqueous medium, we developed special nanoparticles (diameter ≈3.0 nm) which have two independent proton-accepting sites, oxygen or nitrogen atoms. Because of the tiny size and high functionality, the nanoparticles can be uniformly dispersed in water and behave as single dissolved molecules to form a transparent colloidal solution. The synthetic route of the nanoparticles is given in Scheme 1, which is based on hydrolytic condensation of a functionalized precursor, *N*,*N*-di(2,3-dihydroxypropyl)(aminopropyl)triethoxysilane, $(HOCH_2CH(OH)CH_2)_2NCH_2CH_2CH_2Si(OCH_2CH_3)_3$. Although the nanoparticles have a variety of characteristic properties, such as high functionalities, solubility in aqueous medium, and nanometer size, the mechanism of the formation and the precise structure of the nanoparticles are not yet fully understood.

Scheme 1. Synthetic Route for the Nanoparticles Based on Hydrolytic Condensation of a Functionalized Precursor, *N*,*N*-di(2,3-dihydroxypropyl)Aminopropyltriethoxysilane

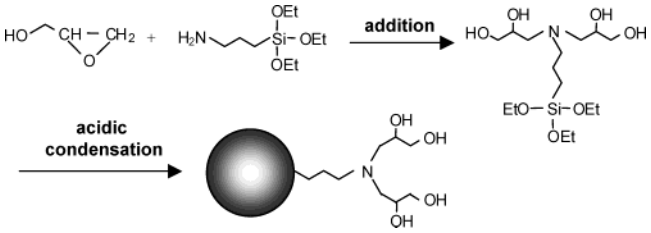

The hydrolysis and polycondensation of substituted alkoxysilanes, $R-Si(OR')_3$, containing a nonhydrolyzable Si−C bond give a variety of silsesquioxanes with various substituent groups and cage structures.[3−5] The term of silsesquioxane indicates a family of compounds characterized by a ratio of 1.5 between the silicon and oxygen atoms.[5] The silsesquioxane family is now recognized to have an enormous potential as a building block for various advanced materials, and their applications can be found in the areas of catalysis, coordination chemistry, and material science, such as organic−inorganic nanocomposites. The structures can be expressed in general formula: $(R-SiO_{1.5})_n$ (n = even number).[6] Completely condensed silsesquioxanes, (R−

* To whom correspondence should be addressed. E-mail: h.mori@yz.yamagata-u.ac.jp; phone: +81-238-26-3765; fax: +81-238-26-3092.

† Present address: Department of Polymer Science and Engineering, Faculty of Engineering, Yamagata University, 4-3-16, Jonan, Yonezawa, 992-8510, Japan.

‡ Dedicated to the memory of Dr. Michael G. Lanzendörfer.

10.1021/ma035482o CCC: $27.50
Published on Web 06/03/2004

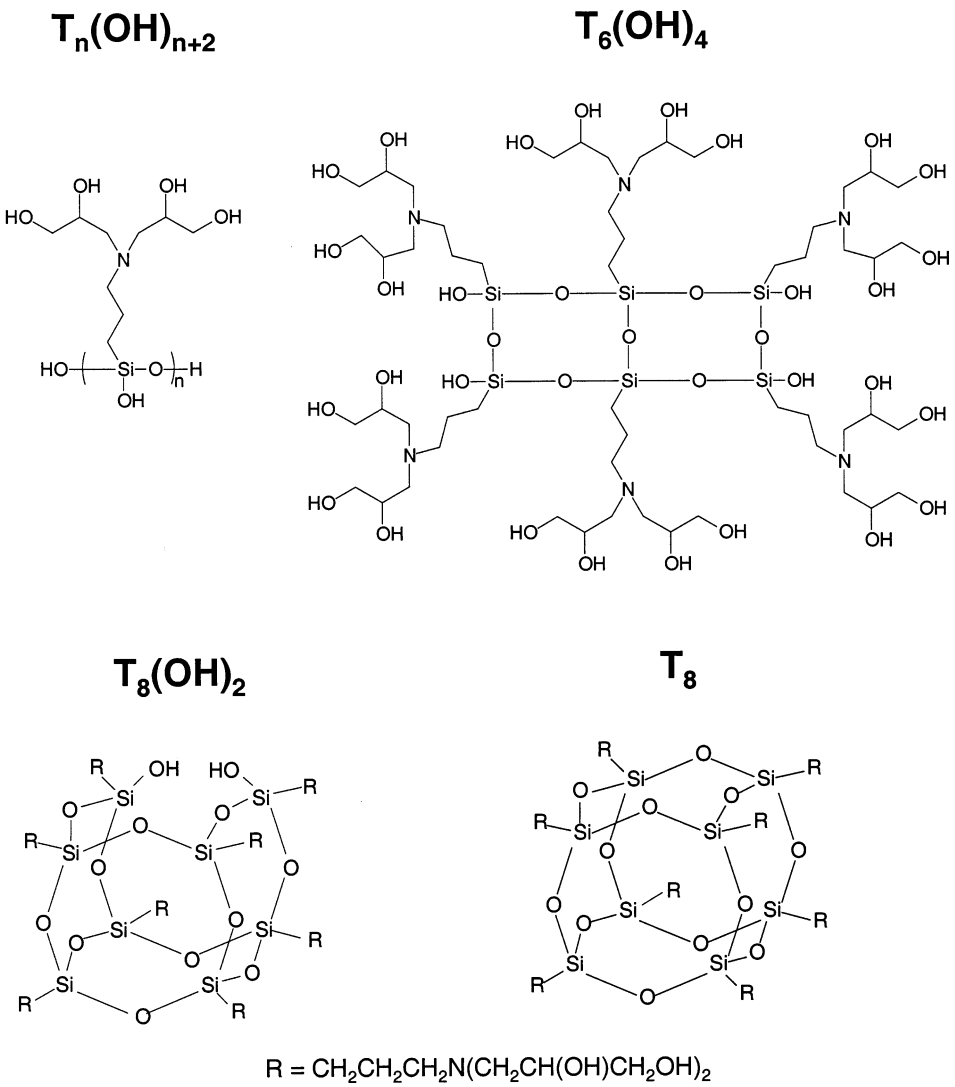

Figure 1. Schematic representation of various structures; linear ($T_n(OH)_{n+2}$), ladder ($T_6(OH)_4$), partially cage ($T_8(OH)_2$), and cage (T_8) structures.

$SiO_{1.5})_n$ with n = 4, 6, 8, 10, and 12, have been synthesized and characterized.[5] Among them, much interest has been paid to cubic $(RSiO_{1.5})_8$, consisting of a rigid, crystalline silica-like core that is perfectly defined spatially (0.5−0.7 nm) and that can be linked covalently to eight R groups.[7,8] Completely condensed structures with $n > 12$ are not so common but some examples have been reported.[4,9,10] In addition to the fully condensed structures, $(RSiO_{1.5})_n$, which are denoted as T_n (n = even number), incompletely condensed structures containing Si−OH groups are known, which have generic formula $[RSiO_{1.5-x}(OH)_{2x}]_n$ or $T_n(OH)_m$.[5,6,11] The structures include perfect polyhedra, incompletely condensed polyhedra (species with one to three OH per molecule), ladder-type structure (species with four OH per molecule), open structure (species with more than five OH per molecule), linear structure, and all their possible combinations. Examples of possible structures are shown in Figure 1.

Recently, several efforts have been directed at the preparation of novel colloids and nanoparticles on the basis of the hydrolytic condensation of monosilanes, and the resulting products are often called as polysilsesquioxanes colloids or polyorganosiloxane nanoparticles. For example, Brostein et al. reported the synthesis of a new family of polysilsesquioxanes colloids based by hydrolytic condensation of *N*-(6-aminohexyl)aminopropyltrimethoxysilane, $H_2N(CH_2)_6NHCH_2CH_2CH_2Si(OCH_3)_3$.[12] They claimed that the well-defined colloids (30−50 nm) were obtained at neutral initial pH. Ma et al. demonstrated the synthesis of nanoparticles of poly(phenyl/methylsilsesquioxane) by emulsion polymerization of a cohydrolyzate from a mixture of trichlorophenylsilane and trichloromethylsilane.[13] The average size of the resultant particles could be controlled from 30 to 250 nm in diameter by changing the initial conditions. Poly(phenylsilsesquioxane)s with particle sizes from 30 to 110 nm were also prepared by emulsion polymerization of phenylsilanetriol.[14] The synthesis of colloidal particles was conducted by using alkylalkoxysilanes, in which methyltrimethoxysilane was used as a network-forming monomer and diethoxydimethylsilane was employed as a chain-forming monomer in the presence of the surfactant.[15] They demonstrated that the first step is the base-catalyzed hydrolysis and condensation, followed by saturation of reactive groups at the surface of the grown particles to prevent irreversible aggregation and to prevail single particle properties. The resulting polyorganosiloxane nanoparticles have small size ($2 \leq R \leq 50$ nm), depending on the preparation conditions.

The aim of this study is to understand the precise structure and the formation mechanism of the nano-

particles prepared by the hydrolytic condensation of the functionalized precursor, *N*,*N*-di(2,3-dihydroxypropyl)-(aminopropyl)triethoxysilane. MALDI-TOF analysis enabled us to characterize the nanoparticles, informing the molecular mass and the specific number of silanol groups (and thus, the number of closed ring structures in each chain) as a function of the number of repeat units in the molecule. For 6−10 Si repeat units, the fraction of closed rings formed by an intramolecular cyclization could be determined quantitatively. NMR, FT-IR, and elemental analyses gave information on the structure of the alkyl chain attached on a Si atom and the chemical composition of the nanoparticles, respectively. The particle size and morphology were evaluated by transmission electron microscopy (TEM) and scanning force microscopy (SFM).

Experimental Section

Synthesis. Preparation of the nanoparticles was conducted by addition reaction of (aminopropyl)triethoxysilane and glycidol, followed by acidic condensation of the addition product, as shown in Scheme 1.[2] The first step is the synthesis of *N*,*N*-di(2,3-dihydroxypropyl)-(aminopropyl)triethoxysilane, in which one mole of (aminopropyl)triethoxysilane was dropped slowly into two moles of glycidol under stirring with ice cooling, and then the mixture was reacted for 1 h at 23 °C. The second step is the hydrolytic condensation of the addition product in methanol with aqueous HF solution. To 44.55 g (120.6 mmol) of the adduct dissolved in 200 mL methanol was added 6.727 g of aqueous HF solution (3.225%) under stirring. After the reaction mixture was stirred for an additional 2 h at ambient temperature, water, ethanol, and methanol were removed in a vacuum and the nanoparticles were dried at 40 °C at 8 mbar to give a glassy solid at room temperature. It was changed easily into a highly viscous transparent material by heating, for example, at 60 °C. The resulting nanoparticle is soluble directly in water, methanol, DMF, and DMSO, while insoluble in most organic solvents, such as dichloromethane, acetone, and dioxane, etc.

Instrumentation. ^{1}H and ^{13}C NMR spectra were recorded with a Bruker AC-250 spectrometer. The ^{29}Si NMR spectrum was obtained using a Bruker AMX-250 spectrometer. The ^{29}Si NMR measurement of the silsesquioxane-based nanoparticles was conducted in DMSO-d_6 (1.5 g nanoparticles per mL solvent) at 49.7 MHz, using inverse gated sequence, a pulse angle of 30°, a relaxation delay of 2 s, and a number of scans of 2046 and TMS as a reference. FT-IR spectra were recorded on a Bruker Equinox 55 spectrometer. The sample of the nanoparticles was obtained by casting a methanol solution on NaCl plates. The elemental analyses were performed by Ilse Beetz Mikroanalytisches Laboratorium (Kulmbach). Bright field transmission electron microscopy (TEM) was performed using a Zeiss electron microscope (CEM 902) operated at 80 kV. The samples for TEM observation were prepared by applying a drop of a diluted DMF solution (10 mg/L) on carbon-coated Cu grids and allowed to dry in air. Scanning force microscopy (SFM) height and phase images were taken on a Digital Instruments Dimension 3100 microscope operated in tapping mode (free amplitude of the cantilever ≈30 nm, set point ratio ≈0.98). The samples were prepared on polished silicon wafers by dip-coating from DMF, methanol, and aqueous solutions (1 mg/100 mL), respectively.

MALDI-TOF mass spectroscopic analysis was performed on a Bruker Reflex III equipped with a 337 nm N_2 laser in the reflector mode and 20 kV acceleration voltage. To find a suitable condition, various matrixes, such as 5-chlorosalicylic acid (Aldrich 98%), 2,5-dihydroxybenzoic acid (Aldrich 99%), α-cyano-4-hydroxy cinnamic acid (Sigma), 2-(4-hydroxyphenylazo)benzoic acid (Fluka >99.5%), *trans*-3-(3-indolyl)acrylic acid (Aldrich 99%), hydroxypicolinic acid (98%), picolinic acid (Aldrich 99%), and sinapic acid (Fluka >99%), were screened in the presence and absence of a salt. Sodium trifluoroacetate (NaTFA, Fluka, 99.5%) was used as a salt for ion formation. However, the samples without salt showed better signals in all cases. Samples were prepared from methanol solution by mixing matrix (20 mg/mL) and the silica (10 mg/mL) in a ratio of 10:1. The number-average molecular weights, M_n, of the samples were determined in the linear mode.

Results and Discussion

MALDI-TOF MS Analysis. Recently, MALDI-TOF MS has become a very powerful tool for the investigation of siloxane,[16] silsesquioxane,[17,18] and organic molecules on silicon[19] and silica[20] surfaces. In this study, MALDI-TOF MS was used for the determination of the molecular weights, molecular weight distribution, and the detailed structures. We found that several matrixes, 2-(4-hydroxyphenylazo)benzoic acid, α-cyano-4-hydroxy cinnamic acid, *trans*-3-(3-indolyl)acrylic acid, and sinapic acid, could be used for the analysis, and all samples showed a unimodal symmetrical peak. In all cases, the samples without salt showed better signals.

Figure 2a shows the MALDI-TOF MS of the nanoparticles measured by linear mode using 2-(4-hydroxyphenylazo)benzoic acid as a matrix. From the signal, $M_n = 3760$ and $M_w/M_n = 1.08$ could be obtained. The kind of the matrix had no significant influence on the MALDI-TOF MS results. Assuming the formation of the silsesquioxane where each silicon atom is bound to an average of one and a half oxygens and to one alkyl chain, the theoretical molecular weights of silsesquioxane, $(RSiO_{1.5})_n$, can be calculated to be 3096, 3612, 4128, and 4644 g/mol for $n = 12$, 14, 16, and 18, respectively. As shown in the next section, the actual product consists of many species having 12−18 Si atoms and different number of intramolecular cyclizations.

Figure 2b shows MALDI-TOF MS of the nanoparticles measured by reflector mode, which leads to enhance the resolution. The sample was prepared using sinapic acid as a matrix without salt. The overall shape of the unimodal peak distribution is similar to that measured by linear mode. Figure 3a shows mass spectrum in the 1450−1850 *m*/*z* range for the silsesquioxane-based nanoparticles. Two major peaks are seen at 1515.7 and 1782.7 *m*/*z*, respectively. The nominal separation between these major peaks, 267.0 g/mol, is equal to the repeat group, $RSiO_2H$ (theoretical value = 267.35 g/mol, where $R = CH_2CH_2CH_2N(CH_2CH(OH)CH_2OH)_2$) of linear and branched structures. As shown in Figure 1, the repeat group has two Si−O−Si bridges and one unreacted −SiOH group per repeat group, which is generally indicative of a branched-linear material. The difference is ascribed to the species having different number of Si atoms formed by an intermolecular reaction of −SiOH groups. The nominal spacing of 267.0 g/mol also indicates that the nanoparticles are singly charged.

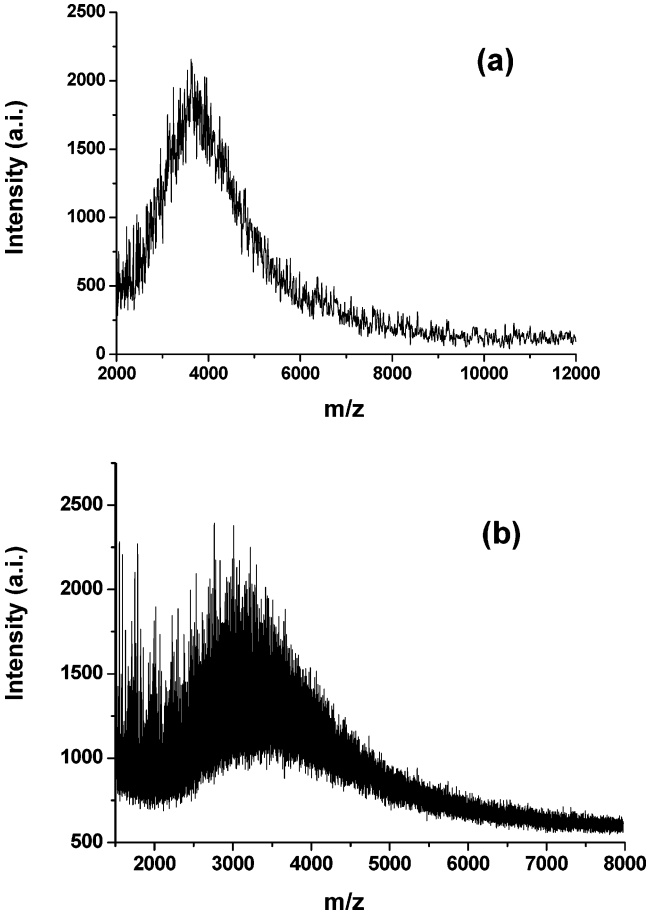

Figure 2. MALDI-TOF mass spectra of the nanoparticles measured by (a) linear mode using 2-(4-hydroxyphenylazo)-benzoic acid as a matrix and by (b) reflector mode using sinapic acid.

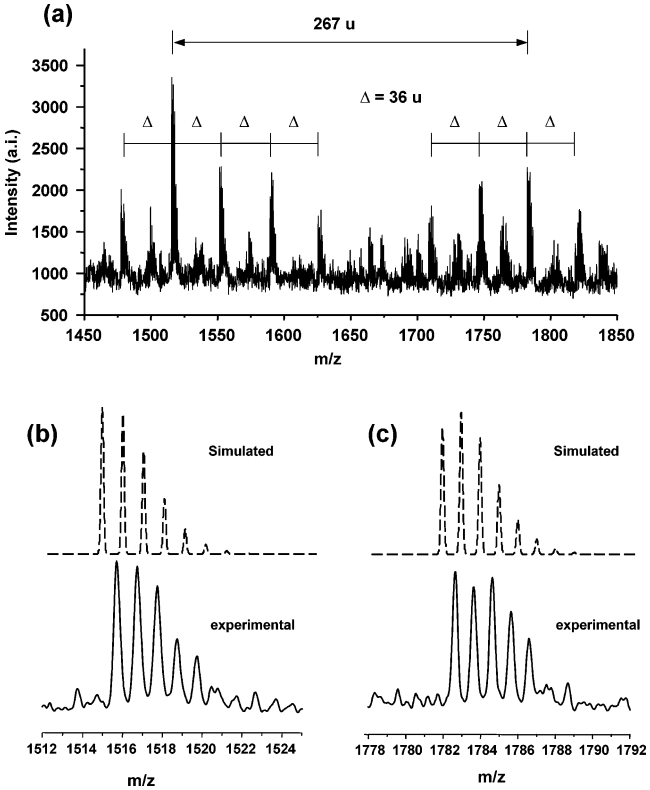

Figure 3. MALDI-TOF mass spectrum of the nanoparticles in the 1450−1850 *m*/*z* range (a), experimental and calculated isotopic patterns of MALDI-TOF signal at *m*/*z* = 1515.1 (b), and *m*/*z* = 1782.4 (c).

Many peaks having moderate intensities, which are up to about 50% of the maximum value observed at *m*/*z* = 1515.7, are detected around the two major peaks (Figure 3a). The distance between these peaks is 36 g/mol, indicating the loss of two water molecules. Actually, less intense peaks (about 20−50% of the maximum peak) are seen successively (see the Supporting Information, Figure S1) and the subdistribution shifted by 18 g/mol with respect to the distribution of the moderate peaks is clearly due to the loss of a water molecule. This reaction can occur when two dangling −SiOH groups in close proximity within a given molecule react intramolecularly to form a Si−O−Si bridge. When such an intramolecular reaction occurs, a closed loop can be formed in the molecule. The peak-to-peak spacing of 18 g/mol must result from an intramolecular reaction, because an intermolecular reaction of this type should result in a shift of a multiple of 267.35 g/mol, leading to the formation of other species having different number of Si atoms.

Tables 1−3 show the assignment of the main peaks appearing in the mass spectra. General structures for three-dimensional silsesquioxanes involve polyhedral-type, ladder-type, branched, and linear structures. The essential difference between these structures is the level of −SiOH condensation. The degree of intramolecular condensation was established for every member of the series of oligomers.[21,22] For the condensation products derived from the alkyltriethoxylsilane, $R-Si(OEt)_3$, considered here, the mass *m* of the linear and branched products having *n* repeat groups is given by the equation

$$m = (267.35\ n) + p + 18 \qquad (1)$$

where *n* is the number of repeat groups (which is equal to the number of Si atoms per product), *p* is the mass of the cation (either 23 g/mol for sodium or 1 g/mol for proton), and 18 g/mol is for the two $O_{1/2}H$ end groups. On the other hand, for the species formed by intramolecular ring formation, the following equation is given

$$m = (267.35\ n) + p - (18t) + 18 \qquad (2)$$

where again *n* is the number of repeat groups, *p* is the mass of the cation, *t* is equal to the number of closed loops in the molecules, and 18 g/mol is for the added end groups. As can be seen in Tables 1−3, a series of *t* values were present for particular *n* values ($t = 0\sim8$ at $n = 6$, $t = 2\sim10$ at $n = 7$, and $t = 4\sim13$ at $n = 8$). Hence, the MALDI-TOF MS gave information on a primary distribution of species characterized by the number of Si atoms in their structures (*n*) and a secondary distribution giving the fraction of species with different values of *t* for a constant value of *n*. A characteristic fraction of intramolecular cycles at a specific *n* value can be expressed by using the value of *t* for the species showing the highest intensity. The major peaks observed at 1515.7 and 1782.7 *m*/*z* are assigned to the species having $n = 6$ and $t = 6$ and $n = 7$ and $t = 6$, respectively, ionized with H^+ (theoretical values for the isotropic composition are 1515.1 and 1782.4 g/mol, respectively).

The presence of several peaks around the average theoretical value is due to the isotopic distribution. As can be seen in Figure 3b and c, the calculated isotopic

Table 1. Assignment of MALDI-TOF MS Peaks in the Range of 1400−1700 *m/z*

m/z (exp.)	species[a]	structure[b] $T_n(OH)_m$	*f* [c]	*m/z* (theor.)
1477.8	$n = 6$, $t = 8$	T_6-4(H_2O) = $T_6(OH)_8$-8(H_2O)	2.0	1479.0 (+ H^+)
1497.8	$n = 6$, $t = 7$	T_6-3(H_2O) = $T_6(OH)_6$-6(H_2O)	1.75	1497.0 (+ H^+)
1515.7	$n = 6$, $t = 6$	T_6-2(H_2O) = $T_6(OH)_4$-4(H_2O)	1.5	1515.1 (+ H^+)
1532.7	$n = 6$, $t = 5$	T_6-1(H_2O) = $T_6(OH)_2$-2(H_2O)	1.25	1533.1 (+ H^+)
1551.7	$n = 6$, $t = 4$	T_6	1.0	1551.1 (+ H^+)
1571.7	$n = 6$, $t = 3$	$T_6(OH)_2$	0.75	1569.1 (+ H^+)
1573.7	$n = 6$, $t = 4$			1573.1 (+ Na^+)
1587.7	$n = 6$, $t = 2$	$T_6(OH)_4$	0.5	1587.1 (+ H^+)
1592.7	$n = 6$, $t = 3$			1591.1 (+ Na^+)
1625.7	$n = 6$, $t = 0$	$T_6(OH)_8$	0	1623.2 (+ H^+)
	$n = 6$, $t = 1$			1627.2 (+ Na^+)

[a] Definition of species according to eq 2; $m = (267.35n) + p - (18t) + 18$, where n is the number of repeat groups, p is the mass of the cation, t is equal to the number of closed loops in the molecules. [b] Structure according to eq 3. [c] Fraction of intramolecular cycles (f) according to eq 4; $f = (2 + n - m)/(2 + n)$.

Table 2. Assignment of MALDI-TOF MS Peaks in the Range of 1700−1900 *m/z*

m/z (exp.)	species[a]	structure[b] $T_n(OH)_m$	*f* [c]	*m/z* (theor.)
1708.6	$n = 7$, $t = 10$	$T_7(OH)_1$-6(H_2O)	2.5	1710.4 (+ H^+)
1711.7				
1727.7	$n = 7$, $t = 9$	$T_7(OH)_1$-5(H_2O) = $T_7(OH)_9$-9(H_2O)	2.25	1728.4 (+ H^+)
1746.7	$n = 7$, $t = 8$	$T_7(OH)_1$-4(H_2O) = $T_7(OH)_7$-7(H_2O)	2.0	1746.4 (+ H^+)
1749.6	$n = 7$, $t = 9$			1850.4 (+ Na^+)
1762.6	$n = 7$, $t = 7$	$T_7(OH)_1$-3(H_2O) = $T_7(OH)_5$-5(H_2O)	1.25	1764.4 (+ H^+)
1782.7	$n = 7$, $t = 6$	$T_7(OH)_1$-2(H_2O) = $T_7(OH)_3$-3(H_2O)	1.5	1782.4 (+ H^+)
1799.8	$n = 7$, $t = 5$	$T_7(OH)_1$-1(H_2O)	1.25	1800.4 (+ H^+)
1804.6	$n = 7$, $t = 6$			1804.4 (+ Na^+)
1818.6	$n = 7$, $t = 4$	$T_7(OH)_1$	1.0	1818.4 (+ H^+)
1836.7	$n = 7$, $t = 3$	$T_7(OH)_3$	0.75	1836.4 (+ H^+)
1856.6	$n = 7$, $t = 2$	$T_7(OH)_5$	0.5	1854.4 (+ H^+)
	$n = 7$, $t = 3$			1858.4 (+ Na^+)

[a] Definition of species according to eq 2. [b] Structure according to eq 3. [c] Fraction of intramolecular cycles (f) according to eq 4; $f = (2 + n - m)/(1 + n)$.

Table 3. Assignment of MALDI-TOF MS Peaks in the Range of 1900−2200 *m/z*

m/z (exp.)	species[a]	structure[b] $T_n(OH)_m$	*f* [c]	m/z (theor.)
1919.7	$n = 8$, $t = 13$	T_8-8(H_2O)	2.6	1923.7 (+ H^+)
1939.7	$n = 8$, $t = 12$	T_8-7(H_2O)	2.4	1941.7 (+ H^+)
1955.7	$n = 8$, $t = 11$	T_8-6(H_2O)	2.2	1959.7 (+ H^+)
1975.7	$n = 8$, $t = 10$	T_8-5(H_2O) = $T_8(OH)_{10}$-10(H_2O)	2.0	1977.8 (+ H^+)
1993.7	$n = 8$, $t = 9$	T_8-4(H_2O) = $T_8(OH)_8$-8(H_2O)	1.8	1995.7 (+ H^+)
2013.7	$n = 8$, $t = 8$	T_8-3(H_2O) = $T_8(OH)_6$-6(H_2O)	1.6	2013.8 (+ H^+)
2031.7	$n = 8$, $t = 7$	T_8-2(H_2O) = $T_8(OH)_4$-4(H_2O)	1.4	2031.8 (+ H^+)
2049.7	$n = 8$, $t = 6$	T_8-1(H_2O) = $T_8(OH)_2$-2(H_2O)	1.2	2049.8 (+ H^+)
2067.7	$n = 8$, $t = 5$	T_8	1.0	2067.8 (+ H^+)
2086.7	$n = 8$, $t = 4$	$T_8(OH)_2$	0.8	2085.8 (+ H^+)

[a] Definition of species according to eq 2. [b] Structure according to eq 3. [c] Fraction of intramolecular cycles (f) according to eq 4; $f = (2 + n - m)/(2 + n)$.

distributions corresponding to these two major structures consist of a set of isotopically resolved individual peaks. These patterns are consistent in the margin of error with the experimentally observed distributions. In the most cases, a reasonable agreement was found between the experimental molar mass and predicted value, ionized with H^+, as indicated in Tables 1−3. However, a slight difference between the calculated and experimental values was observed in some species. One possible reason for the shift is due to a very close concentration of different isotopes in the range of average values. Some experimental signals are assigned to species overlapped by H^+-ionized and Na^+-ionized products. Figure 4 shows the isotopic distribution corresponding to T_8 structure, as H^+ and Na^+ adducts. The overlapping two isotopic patterns are contributed to each experimental signal. The same series of signals as in the H^+-ionized samples is considered to be obtained in Na^+-ionized products. The mass difference between Na^+ and H^+ is 22 g/mol, which is close to that of one water molecule (18 g/mol). In some areas, the signals of the Na^+-ionized samples may have reasonable intensities, which are comparable to the H^+-ionized samples having one additional water molecule. Nevertheless, reasonable peaks having peak-to-peak spacing of 18 g/mol were observed until $m/z \sim 2600$ (see the Supporting Information, Figure S2).

The presence of a certain concentration of the species having Si−OH groups suggests that the hydrolysis proceeds with a much higher rate than the condensation. This is consistent with the general tendency of hydrolytic condensation, in which the first step (the hydrolysis of the monosubstituted silane to give corresponding trisilanol) is faster than that of the second step.[5] The condensation of trisilanol is regarded as the second step, which is a multistep process involving the formation of many different intermediate structures. The species having less number of intermolecular cyclization ($t = 0\sim2$ at $n = 9$ and $t = 0\sim4$ at $n = 10$, respectively) could not be detected (see the Supporting Information, Tables S1 and S2), indicating that the probability of the unreacted Si−OH groups decreases

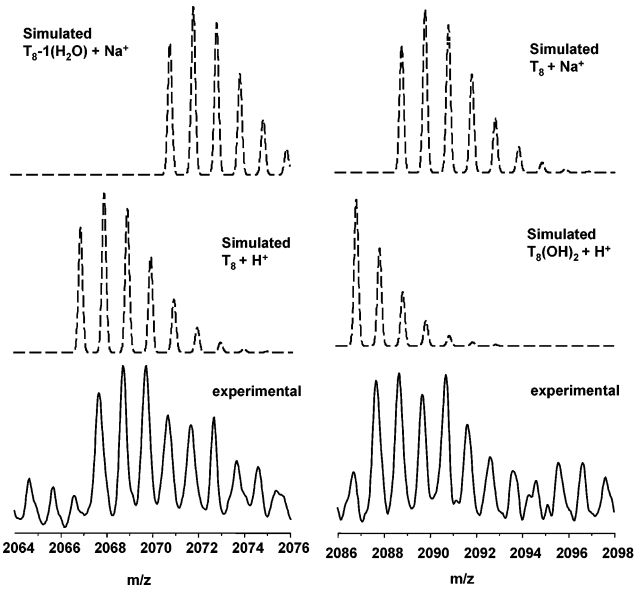

Figure 4. Experimental and calculated isotopic patterns of MALDI-TOF signals in the ranges of (a) 2064−2076 and (b) 2086−2098 *m*/*z*.

with increasing the number of Si atoms. It means that the species with more OH groups condensed with higher probability, giving place to a next generation of products consisting of more Si atoms. Hence, the main products having 12−18 Si atoms may contain less number of linear and open structures, and most probably consists of complete and incomplete cagelike structures.

In the cases of fully condensed structures, perfect polyhedral of formula, $(RSiO_{1.5})_n$, is denoted as T_n (n = even number). Whereas, partially hydrolyzed/condensed products have the general formula $T_n(OH)_x(OR')_y$ where $T = RSiO_{1.5-m/2n}$, and $m = x + y$.[5,6,11] Assuming complete hydrolysis or condensation of alkoxy groups, incompletely condensed structures containing Si−OH groups, $[RSiO_{1.5-x}(OH)_{2x}]_n$, have a general formula

$$T_n(OH)_m \tag{3}$$

where $m = 0, 2, 4,..., (2 + n)$ for n = even number and $m = 1, 3, 5,..., (2 + n)$ for n = odd number. At $m = 0$, the structure corresponds to completely condense polyhedral. The maximum value of m is equal to $2 + n$, representing a linear/branched chain without any intramolecular cycles. The maximum number of intramolecular cycles is equal to $(2 + n)/2$ (for n = even) or $[(2 + n) - 1]/2 = (1 + n)/2$ (for n = odd), whereas the actual number is $[(2 + n) - m]/2$. Therefore, the fraction of intramolecular cycles (f) of a generic n-mer is given by[23]

$$f = (2 + n - m)/(2 + n) \text{ (for } n = \text{even)}$$

or

$$f = (2 + n - m)/(1 + n) \text{ (for } n = \text{odd)} \tag{4}$$

This approach has been used to characterize the fraction of intramolecular cycles in various silsesquioxane from open structures (which is a limit of linear/branched chains, $f = 0$) to closed structures (limit of completely condensed polyhedra, $f = 1$). Some experimental signals observed in MALDI-TOF MS exceed the limitation of completely condensed polyhedra ($f = 1$). For example, the values of intramolecular cycles fraction (f) of two major peaks observed at 1515.7 and 1782.7 *m*/*z*, which correspond to T_6-2(H_2O) and $T_7(OH)_1$-2(H_2O), are 1.5 in both cases. This clearly indicates that some of the hydroxyl groups in the alkyl chain attached on Si atom take part in the hydrolysis−condensation reaction and at least two intramolecular Si−O−C bonds are formed, in addition to the Si−O−Si bonds. Similar phenomenon including the formation of Si−O−C bonds was reported on hydrolytic condensation of an organotrialkoxysilane with a bulky organic group bearing hydroxyl functionalities, in the presence of both acid and basic catalysts.[24,25] The starting silane was a reaction product of *N*-(2-aminoethyl)-3-aminopropyltrimethoxysilane with three moles of phenylglycidyl ether, which has three secondary hydroxyl groups in the precursor. They claimed that the narrow distribution of perfect and imperfect polyhedra, T_8, $T_9(OH)$, and T_{10}, with traces of $T_7(OH)$ and $T_{11}(OH)$ could be obtained, which may be due to the presence of a bulky organic substituent (steric effect promoting intramolecular condensation).

Every species present in the lower molar mass range, T_6-[1∼4(H_2O)], $T_7(OH)_1$-[1∼5(H_2O)], and T_8-[1∼5(H_2O)], can translate to $T_n(OH)_m$-mH_2O in our system. This means that all silanol groups can react with hydroxyl groups, and the products can consist of m Si−O−C and remaining Si−O−Si bonds without any Si−OH groups. From another point of view, among four hydroxyl groups (two secondary and two primary hydroxyl groups) attached to one organic chain, at maximum 1.2−1.4 hydroxyl groups (1.33 for $T_6(OH)_8$-8H_2O, 1.29 for $T_7(OH)_9$-9H_2O, 1.25 for T_8 $(OH)_{10}$-10H_2O, which can be calculated by m/n in the formula $T_n(OH)_m$-mH_2O) can participate to the formation of Si−O−C bonds, and other hydroxyl groups should be kept without change during the hydrolytic condensation. These results also indicate the difficulty in keeping the intact hydroxyl groups under the condition used for the production of the nanoparticles. Nevertheless, it was confirmed that the resulting nanoparticles still have high OH functionality, that is, 16 OH groups in T_6-4(H_2O), 16 OH groups in T_8-8(H_2O), 22 OH groups in T_{10}-9(H_2O). The formation of Si−O−C bonds through the reaction of SiOH (or SiOEt) groups with the hydroxyl functionalities of an organic moiety bonded to a neighboring Si atom can produce intramolecular cycles, while the intermolecular reaction leads to production of other species having different number of Si atoms. This in turn indicates the possibility to produce an organic−inorganic network based on Si−O−C bonds as well as an inorganic network (Si−O−Si).

Assuming that the secondary and primary hydroxyl groups have comparable reactivity toward SiOH (or SiOEt), two possible structures of the key species, T_6-2(H_2O), can be drawn (Figure 5). These structures basically rely on the intramolecular cyclization to form new eight-membered rings. In addition, a variety of structures may be possible, and some of them should be related with the final products consisting of 12−18 Si atoms. Unfortunately, the precise characterization of species having higher molar mass was unsuccessful in this study, which may be due to the overlapping various species. As mentioned in the Introduction, some examples of completely condensed structures, $(R-SiO_{1.5})_n$ with $n > 12$, have been reported,[4,9,10] and some representative structures are shown in Figure 6. For example, Agaskar and Klemperer have demonstrated that hydridosilsesquioxanes, $(HSiO_{1.5})_n$, where polyhe-

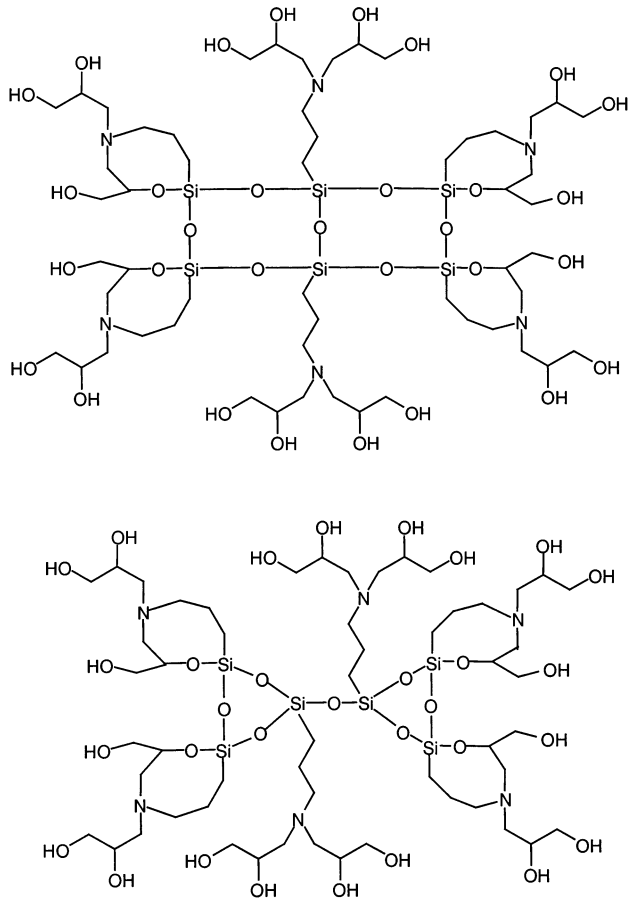

Figure 5. Possible structures for the key species, T_6-2(H_2O).

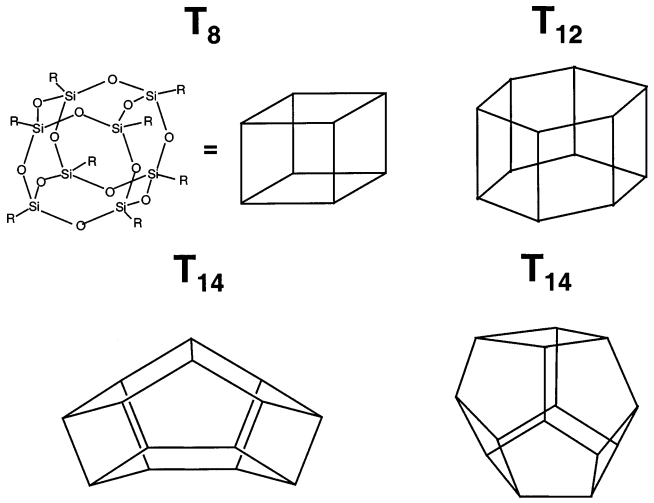

Figure 6. Examples of possible structures of T_8, T_{12}, and T_{14}.

dra with n = 8, 10, 12, 14, 16, and 18 have been isolated.[26] They have also succeeded to collect pure two isomers of $(HSiO_{1.5})_{14}$ and to determine the structures (T_{14} in Figure 6) by X-ray diffraction method.[9] Cage-rearrangement from octa-silsesquioxanes, $(RSiO_{1.5})_8$, to deca- and dodeca-silsesquioxane cages, $(RSiO_{1.5})_{10}$ and $(RSiO_{1.5})_{12}$, has been also reported.[27] Silsesquioxanes, $(RSiO_{1.5})_{12}$, have been obtained in small amounts from the hydrolytic condensation of monosilanes.[9,28,29] Two unstrained structures are known; one has the shape of a prism with six distorted-square faces and two distorted-hexagonal faces (T_{12} in Figure 6); the other has four distorted square-triangler faces and four distorted-pentagonal faces. Theoretical calculation showed two isomeric structures have the same energies.[30] Recent theoretical study on the total energies of completely condensed silsesquioxanes having different sizes indicated that the cubic $(HSiO_{1.5})_8$ has a similar energy to those of the silsesquioxanes with higher n values (n > 8).[30,31] All of these researches suggest the feasibility to produce silsesquioxanes with higher n = 12−18.

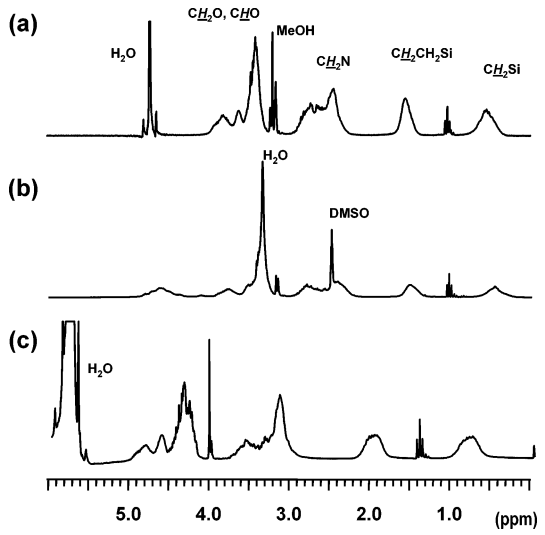

Figure 7. ^1H NMR spectra of the nanoparticles in (a) CD_3OD, (b) DMSO-d_6, and (c) D_2O.

NMR, FT-IR, and Elemental Analyses. ^1H and ^{13}C NMR analyses provide useful information for the characterization of silsesquioxane species, in particular the structure of alkyl group attached on silicon atoms. Although drawing straight conclusions from such spectra is not obvious because of the existence of various species as discussed in MALDI-TOF MS analysis, some indications of the most probable structures may be obtained. Figure 7 shows ^1H NMR spectra of the nanoparticles measured in different solvents (D_2O, d-DMSO, CD_3OD). All ^1H NMR spectra show broad resonances, indicating that the mobility of the alkyl chain is significantly constrained because of the covalently attachment to the surfaces of the nanoparticles. In the measurement in CD_3OD, the peaks corresponding to alkyl chains are present at 0.3−0.8 (CH_2 in the α position to the Si atom), 1.3−1.7 (CH_2 in the β position to the Si atom), 2.2−3.0 (CH_2 in the α position to the N atom), and 3.3−4.0 (CH_2 and CH in the α position to the O atom). The peaks attributed to the alkyl chain are detected with slight shifts in D_2O and d-DMSO. ^1H NMR is generally useful for establishing the number of silanols, both hydrogen-bonded (δ = 5−7.5) and isolated (δ = 2−4).[3,5] The ^1H NMR spectra of the nanoparticles exhibit no peak at >5 ppm, independent of the nature of the solvent. Furthermore, no extra protons are detected other than the expected quantities, suggesting that the significant amounts of SiOH groups are not present in the products.

Figure 8 shows ^{13}C NMR spectrum of the nanoparticles in CD_3OD. Methylenic carbons in the α- and β-position to the Si atom are observed at δ = 5−12 and 15−22, respectively. These peaks are partially broad, which is due to reduced reorientational mobility close to the Si framework. A multiplicity of peaks corresponding to methylene carbons in the α-position with respect

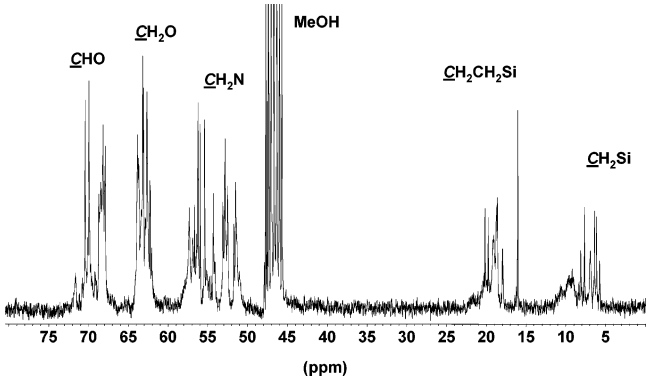

Figure 8. ^{13}C NMR spectrum (CD_3OD) of the nanoparticles.

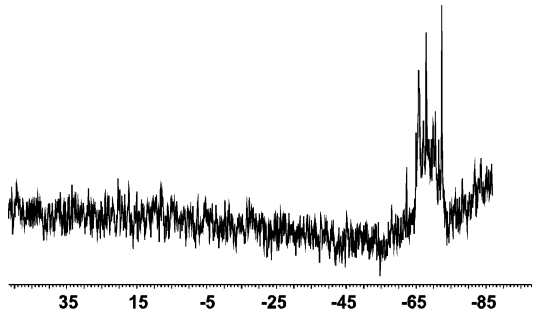

Figure 9. ^{29}Si NMR spectrum (DMSO-d_6) of the nanoparticles.

to amino groups (α-N methylenic carbons) is observed in the range of 50−59 ppm. Methylene carbons associated with CH_2−OH resonances also exhibit many lines in the range of 61−65 ppm. At lower field, methine >CH−OH is observed, also split into many lines (δ = 67−72). The complex distribution of the respective areas of these lines has been observed in various silsesquioxanes. It was generally accepted that the number of the peaks corresponding to a given carbon type, for example, in the α-position to the Si atom, are ascribed to the different type of dissymmetry of the incompletely or completely condensed structure.[24,32,33] The multiplicity is also connected with the different structures of alkyl chains[34−36] and the number of diastereoisomers.[3,24] In our nanoparticles, in addition to such possible multiplicity, the formation of Si−O−C bonds through the reaction of SiOH (or SiOEt) groups with the hydroxyl functionalities of an organic moiety may contribute to the complex distribution.

^{29}Si NMR spectroscopy was also used to characterize the silsesquioxane-based nanoparticles. As can be seen in Figure 9, a series of sharp peaks is observed in the range of −65 to −75 ppm. In general, peaks at lower shift are due to Si connected to other Si atoms through oxygen bridges (−68 to −70 ppm), while peaks of Si atoms linked to an OH group are at higher shift (around −60 ppm).[5] Hence, the result from ^{29}Si NMR suggests that the content of silanol groups in the product is below the detection limit, and therefore the main structures are fully condensed silsesquioxanes, $(R-SiO_{1.5})_n$. The broad peak may be due to ladder- or cagelike structures with higher molecular weight, while the multiplicity of the sharp lines suggests the presence of various species with lower molar mass range, which is consistent with the results of MALDI-TOF MS.

On the basis of the preparation method (acidic condensation of the alkyltriethoxysilanes, $R-Si(OEt)_3$), the general structure of the nanoparticles is expected to be $(R-SiO_{1.5})_n$, where each silicon atom is bound to an average of one-and-a-half oxygens and to one alkyl chain. The structure of the constitutional unit is supported by the result of elemental analysis; the observed atomic composition of the nanoparticles (C, 43.75; H, 7.86; Si, 10.98; N, 4.76) is in fairly agreement with the value (C, 41,86; H, 7.75; Si, 10.85; N, 5.43) calculated from the structure, $R-SiO_{1.5}$ ($R = CH_2CH_2CH_2N(CH_2CH(OH)CH_2OH)_2$). The structure of the constitutional unit in the nanoparticles is the same as that of silsesquioxanes, $(R-SiO_{1.5})_n$. On the basis of the consideration that the term of silsesquioxane indicates a family of compounds characterized by a ratio of 1.5 between the silicon and oxygen atoms,[5] it is entirely fair to say that the product obtained by the hydrolytic condensation of the functionalized precursor is called as "silsesquioxane-based nanoparticles". The nanoparticles may have characteristic properties, which are intermediate between polyhedral silsesquioxanes and silica nanoparticles. Polyhedral silsesquioxanes are often referred to as spherosiloxanes, because polyhedral structures are topologically equivalent to a sphere.

Figures 10 shows FT-IR spectra of the nanoparticles. The OH functionality existing in the alkyl chains is visible as the broad absorption from 3000 to 3800 cm^{-1} with maximum at about 3400 cm^{-1}. In addition, a sharp peak between 2840 and 2940 cm^{-1} is seen, which is due to the C−H stretching vibration in the alkyl chain on the nanoparticles. A strong broad band around 1030−1150 cm^{-1} resulting from Si−O−Si stretching is observed clearly. In the reported characteristic vibrations, the Si−O−Si asymmetric stretching was present at 1100−1140 cm^{-1} or 1057−1085 cm^{-1} in the strained geometry.[4,5] For example, the band for a T_8 is reported at 1121 cm^{-1}, and it is slightly shifted to 1128 cm^{-1} for a T_{10}.[27] Strained cycles as those present in a T_6 show the band at 1051−1057 cm^{-1}.[37] Therefore, it is reasonable to consider that the reaction product obtained by the hydrolytic condensation is a mixture of these species.

SFM and TEM Measurements. Ultrafine particles have lately attracted great attention for various advanced applications. One of the characteristic properties of the nanoparticles prepared in this study is their nanometer-size without any aggregation. In the fields of inorganic nanoparticles, in particular silica particles, many efforts have been paid to control and prevent aggregation and to design of the shape and morphology. One promising way for preventing the aggregation of nanoparticles is to surround them with an appropriate layer, involving various organic molecules and polymers. In our nanoparticles, a high density of functional groups could be attained because each silicon atom should be bound to one alkyl chain in the resulting nanoparticles obtained by the condensation. In other words, the organic alkyl layer can help to prevent interparticle attraction, giving unaggregated nanostructures. Transmission electron microscopy (TEM) and scanning force microscopy (SFM) were employed for the characterization of the size and morphology of the nanoparticles.

Figure 11 shows representative TEM micrographs of the nanoparticles obtained from dilute DMF colloidal solution. The isolated spherical particles are distributed without any aggregation. The size distribution is relatively small, and the average particle size is 2.7 nm. The size of the cubic core consisting of eight silicon atoms is 0.5−0.7 nm,[8,38] and the species having 12−18 silicon atoms should be bigger than the cubic structure. The

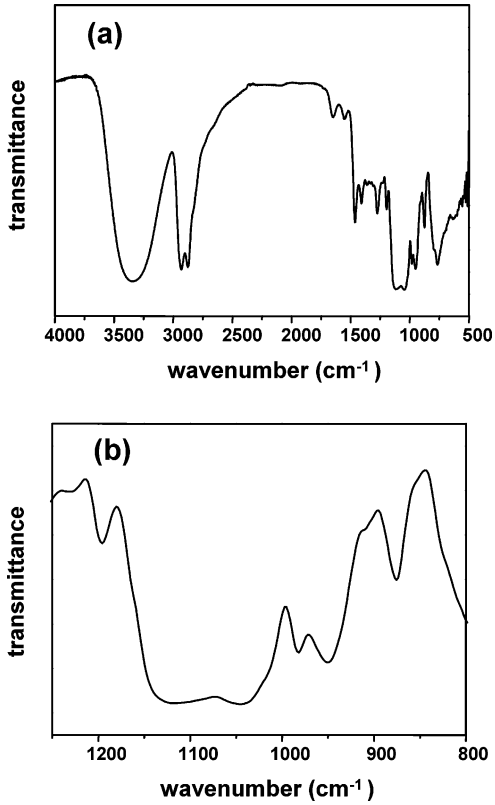

Figure 10. FT-IR spectra of the nanoparticles in the range of (a) 500−4000 cm^{-1} and (b) 800−1250 cm^{-1}.

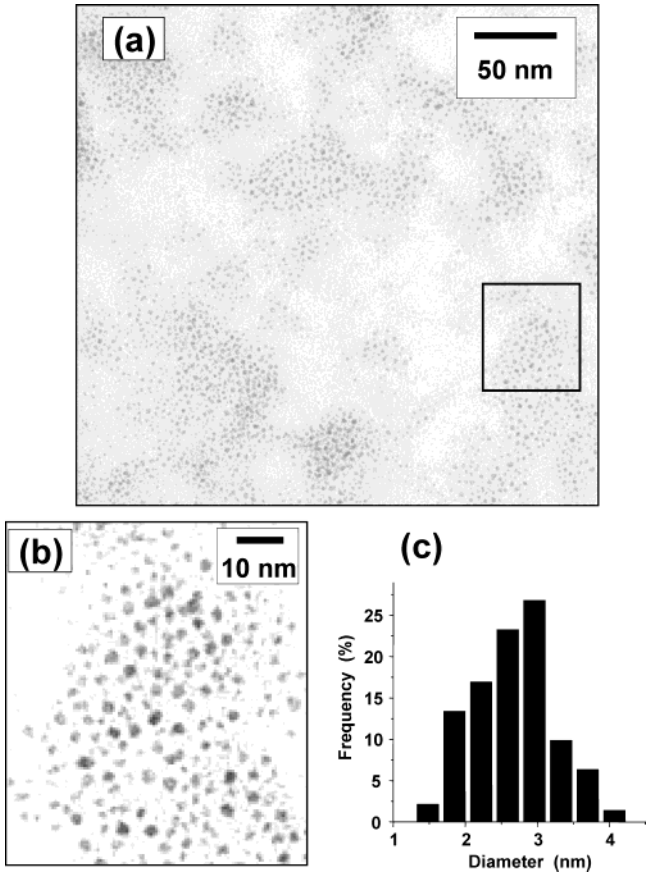

Figure 11. Representative TEM image of the nanoparticles obtained from DMF solution (a), (b) higher magnification image taken from the area inside the box indicated in image (a), and (c) particle size distribution.

length of alkyl chains attached on a silicon atom is expected to be 0.5−1.5 nm, depending on the conformation and crowding. It is assumed the contour length should amount to the sum of four C−C bonds, two C−N bonds, and one O−H bond, if the alkyl chain is in an extended conformation. Hence, it is reasonable to estimate that the particle size measured by TEM corresponds to that of single silsesquioxane-based nanoparticles consisting of 12−18 Si atoms.

For the synthesis of silsesquioxanes by hydrolytic condensation of $R-Si(OR')_3$, the reactions and the resulting structures are influenced by many factors, such as the nature of R′ and R groups, solvent, concentration, the addition rate and quality of water, temperature, pH, and time.[4,5] Among them, water related with the hydrolysis reaction to give trisilanol and the solvent related with the solubility of a precursor may play a relevant role in influencing the synthesis. In our system, since the precursor as well as the resulting nanoparticles are soluble in methanol in the presence of a small amount of HF aqueous solution, the reaction system is homogeneous during the hydrolysis/condensation reaction. This is a quite different feature from conventional systems, in which the reaction is heterogeneous, because precursors containing a H or an alkyl chain bonded to a Si atom are only soluble in organic solvents. In such conventional systems, it is considered that the hydrophobic longer alkyl chains tend to exclude water from reaching the Si−O bonds and thus suppressing the hydrolysis reaction. Steric hindrance may also retard condensation by preventing silanol groups from coming into sufficiently close proximity to allow the elimination reaction to occur. On the other hand, in our system, the long alkyl chain having many hydroxyl groups may support to promote intramolecular cyclization, because of the hydrophilic property. Actually, nanometer size could be achieved by a careful choice of the organic structure and condensation condition. Experiments aiming to evaluate the influences of the reaction conditions and the structure of alkyl chains on the size and morphology of the nanoparticles are currently under way and will be reported elsewhere.

Recently, SFM has been successfully applied to the characterization of a variety of inorganic nanoparticles. In this study, SFM was also employed to visualize the size, shape, and the aggregation states of the nanoparticles. The samples were prepared by dip-coating from DMF, methanol, and aqueous solutions (1 mg/100 mL) using polished silicon wafer as a substrate. Figure 12 shows tapping-mode SFM images of the nanoparticles obtained from various solvents. Spherical particles of about 3 nm in height are observed clearly in the sample prepared from DMF, which are comparable to the size determined by TEM. The same shape and distribution are seen in the phase image (Figure 12b). The apparent phase difference of the nanoparticles from the silicon wafer may stem from the existence of the organic alkyl chains on the nanoparticles. The sample prepared from water also shows spherical nanoparticles having the same nanometer size, suggesting that the nanoparticles can be dispersed on the silicon wafers without aggregation. When the sample was prepared from methanol, aggregated forms of more than 100 nm in height are observed (Figure 12d). Similar aggregation structures were observed in the sample prepared from methanol on a freshly cleaved mica surface, suggesting less influence of the nature of the substrate. For the sample preparation of the heterogeneous materials for SFM

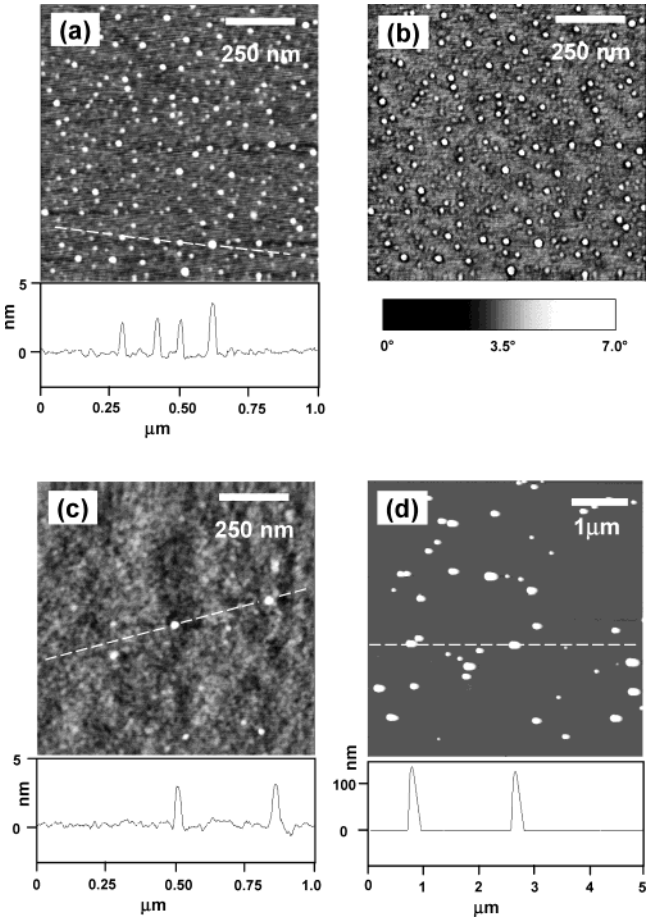

Figure 12. SFM images of the nanoparticles dip-coated from dilute DMF (a, b), H_2O (c), and methanol (d) on Si wafer: (a) height image (*z*-range: 5 nm), (b) phase image (*z*-range: 7°), (c) height image (*z*-range: 5 nm), and (d) height image (*z*-range: 200 nm). Under each height image, we show the cross section at the position indicated by the dotted line.

measurements, it is well known that solvent evaporation can induce mechanical forces that may lead to the destruction of large aggregates formed in solution or, on the contrary, lead to the aggregation. Several authors[39,40] describing SFM imaging for ultrafine particles pointed out that the particles must be bound strongly to the substrate, to prevent them from being swept out by scan of the tip. The visualization of relatively bigger particles formed from methanol solution may come from the mechanical forces, which is stronger than the interaction of the nanoparticles with the substrate during the sample preparation process.

Conclusion

This work present detailed characterization of silsesquioxane-based nanoparticles synthesized by hydrolytic condensation of the functionalized precursor, *N*,*N*-di(2,3-dihydroxypropyl)(aminopropyl)triethoxysilane, $(HOCH_2CH(OH)CH_2)_2NCH_2CH_2CH_2Si(OCH_2CH_3)_3$. It was found that the resulting nanoparticles consist of various species having 12−18 Si atoms with different numbers of intramolecular cyclizations and are comprised mainly of complete and incomplete cagelike structures with not only Si−O−Si bonds but also Si−O−C bonds. The size distribution was relatively small, and the average particle size was 2.7 nm, as confirmed by TEM. The presence of hydroxy groups in the alkyl chain connected to the triethoxysilane facilitates the internal cyclization, and the homogeneous hydrolytic condensation of the precursor may appear to be prerequisite for the nanoparticle formation. Since amino groups (protonated or not) easily interact with various organic species, such as anionic polymers and negatively charged DNA, as well as with the majority of transition-metal compounds, the nanoparticles with tertiary amine groups and hydroxyl groups can be used as a effective building block for a variety of advanced materials.

Acknowledgment. The authors would like to thank the Deutsche Forschungsgemeinschaft (DFG) for financial support. They thank Dr. Oleg Tok for ^{29}Si NMR measurements and A. Göpfert for TEM measurements, respectively.

Supporting Information Available: Figures showing MALDI-TOF mass spectra of the nanoparticles in the ranges of 1450−1600, 1700−1850, 2000−2100, 2200−2300, and 2450−2550 *m*/*z*, and tables giving the assignment of MALDI-TOF MS peaks in the range of 2200−2650 *m*/*z*. This material is available free of charge via the Internet at http://pubs.acs.org.

References and Notes

(1) Sanchez, C.; de Soler-Illia, G. J.; Ribot, F.; Lalot, T.; Mayer, C. R.; Cabuil, V. *Chem. Mater.* **2001**, *13*, 3061−3083.
(2) Mori, H.; Müller, A. H. E.; Klee, J. E. *J. Am. Chem. Soc.* **2003**, *125*, 3712−3713.
(3) Feher, F. J.; Budzichowski, T. A. *Polyhedron* **1995**, *14*, 3239−3253.
(4) Voronkov, M. G.; Lavrent'yev, V. I. *Top. Curr. Chem.* **1982**, *102*, 199−236.
(5) Pescarmona, P. P.; Maschmeyer, T. *Aust. J. Chem.* **2001**, *54*, 583−596.
(6) Eisenberg, P.; Erra-Balsells, R.; Ishikawa, Y.; Lucas, J. C.; Mauri, A. N.; Nonami, H.; Riccardi, C. C.; Williams, R. J. J. *Macromolecules* **2000**, *33*, 1940−1947.
(7) Provatas, A.; Matisons, J. G. *Trends Polym. Sci.* (Cambridge, U.K.) **1997**, *5*, 327−332.
(8) Zhang, C.; Laine, R. M. *J. Am. Chem. Soc.* **2000**, *122*, 6979−6988.
(9) Agaskar, P. A.; Day, V. W.; Klemperer, W. G. *J. Am. Chem. Soc.* **1987**, *109*, 5554−5556.
(10) Frye, C. L.; Collins, W. T. *J. Am. Chem. Soc.* **1970**, *92*, 5586−5588.
(11) Williams, R. J. J.; Erra-Balsells, R.; Ishikawa, Y.; Nonami, H.; Mauri, A. N.; Riccardi, C. C. *Macromol. Chem. Phys.* **2001**, *202*, 2425−2433.
(12) Bronstein, L. M.; Linton, C. N.; Karlinsey, R.; Ashcraft, E.; Stein, B. D.; Svergun, D. I.; Kozin, M.; Khotina, I. A.; Spontak, R. J.; Werner-Zwanziger, U.; Zwanziger, J. W. *Langmuir* **2003**, *19*, 7071−7083.
(13) Ma, C.; Taniguchi, I.; Miyamoto, M.; Kimura, Y. *Polym. J.* (Tokyo) **2003**, *35*, 270−275.
(14) Ma, C.; Kimura, Y. *Polym. J.* (Tokyo) **2002**, *34*, 709−713.
(15) Jungmann, N.; Schmidt, M.; Maskos, M. *Macromolecules* **2001**, *34*, 8347−8353.
(16) Jaumann, M.; Rebrov, E. A.; Kazakova, V. V.; Muzafarov, A. M.; Goedel, W. A.; Moller, M. *Macromol. Chem. Phys.* **2003**, *204*, 1014−1026.
(17) Wallace, W. E.; Guttman, C. M.; Antonucci, J. M. *Polymer* **2000**, *41*, 2219−2226.
(18) Falkenhagen, J.; Jancke, H.; Kruger, R.-P.; Rikowski, E.; Schulz, G. *Rapid Commun. Mass Spectrom.* **2003**, *17*, 285−290.
(19) Wei, J.; Buriak, J. M.; Siuzdak, G. *Nature* (London) **1999**, *399*, 243−246.
(20) Bauer, F.; Sauerland, V.; Glasel, H.-J.; Ernst, H.; Findeisen, M.; Hartmann, E.; Langguth, H.; Marquardt, B.; Mehnert, R. *Macromol. Mater. Eng.* **2002**, *287*, 546−552.
(21) Wallace, W. E.; Guttman, C. M.; Antonucci, J. M. *J. Am. Soc. Mass Spectrom.* **1999**, *10*, 224−230.
(22) Wallace, W. E.; Guttman, C. M.; Antonucci, J. M. *Polymer* **2000**, *41*, 2219−2226.
(23) Eisenberg, P.; Erra-Balsells, R.; Ishikawa, Y.; Lucas, J. C.; Nonami, H.; Williams, R. J. J. *Macromolecules* **2002**, *35*, 1160−1174.

(24) Fasce, D. P.; Williams, R. J. J.; Mechin, F.; Pascault, J. P.; Llauro, M. F.; Petiaud, R. *Macromolecules* **1999**, *32*, 4757−4763.
(25) Fasce, D. P.; Williams, R. J. J.; Erra-Balsells, R.; Ishikawa, Y.; Nonami, H. *Macromolecules* **2001**, *34*, 3534−3539.
(26) Agaskar, P. A.; Klemperer, W. G. *Inorg. Chim. Acta* **1995**, *229*, 355−364.
(27) Rikowski, E.; Marsmann, H. C. *Polyhedron* **1997**, *16*, 3357−3361.
(28) Brown, J. F., Jr.; Vogt, L. H., Jr.; Prescott, P. I. *J. Am. Chem. Soc.* **1964**, *86*, 1120−1125.
(29) Vogt, L. H., Jr.; Brown, J. F., Jr. *Inorg. Chem.* **1963**, *2*, 189−192.
(30) Xiang, K.-H.; Pandey, R.; Pernisz, U. C.; Freeman, C. *J. Phys. Chem. B* **1998**, *102*, 8704−8711.
(31) Earley, C. W. *J. Phys. Chem. A* **2000**, *104*, 6622−6627.
(32) Feher, F. J.; Soulivong, D.; Nguyen, F. *Chem. Commun.* (Cambridge) **1998**, 1279−1280.
(33) Feher, F. J.; Soulivong, D.; Eklund, A. G. *Chem. Commun.* (Cambridge) **1998**, 399−400.
(34) Manson, B. W.; Morrison, J. J.; Coupar, P. I.; Jaffres, P.-A.; Morris, R. E. *J. Chem. Soc., Dalton Trans.* **2001**, 1123−1127.
(35) Liu, C.; Liu, Y.; Shen, Z.; Xie, P.; Dai, D.; Zhang, R.; He, C.; Chung, T. *Macromol. Chem. Phys.* **2001**, *202*, 1576−1580.
(36) Liu, C.; Liu, Y.; Xie, P.; Dai, D.; Zhang, R. *Polym. Adv. Technol.* **2001**, *12*, 475−481.
(37) Brown, J. F., Jr.; Vogt, L. H., Jr. *J. Am. Chem. Soc.* **1965**, *87*, 4313−4317.
(38) Choi, J.; Yee, A. F.; Laine, R. M. *Macromolecules* **2003**, *36*, 5666−5682.
(39) Bourgeat-Lami, E.; Lang, J. *J. Colloid Interface Sci.* **1998**, *197*, 293−308.
(40) Sato, H.; Ohtsu, T.; Komasawa, I. *J. Colloid Interface Sci.* **2000**, *230*, 200−204.

MA035482O